Eur. Phys. J. A **23**, 69–78 (2005)
DOI 10.1140/epja/i2004-10065-1

THE EUROPEAN PHYSICAL JOURNAL A

Coexisting oblate and strongly triaxial structures in ^{191}Pt

T. Kutsarova[1,a], C. Schück[2], E. Gueorguieva[3], A. Minkova[4,1], I. Zartova[4], F. Hannachi[2,b], A. Korichi[2], and A. Lopez-Martens[2]

[1] INRNE-BAS, 1784 Sofia, Bulgaria
[2] CSNSM, IN2P3-CNRS, F-91405 Orsay, France
[3] iThemba Laboratory for Accelerator Based Sciences, P.O. Box 722, Somerset West, South Africa
[4] Faculty of Physics, University of Sofia, 1164 Sofia, Bulgaria

Received: 29 June 2004 /
Published online: 23 November 2004 –
Communicated by D. Schwalm

Abstract. Excited states in ^{191}Pt have been populated using the reaction ^{186}W + ^{11}B at 85 MeV beam energy. Gamma-ray coincidences were measured using the EUROGAM-II spectrometer array. The level scheme has been extended considerably. Evidence for favoured structures of highly triaxial shape with $\gamma \sim -90^\circ$ coexisting with oblate structures has been obtained by comparison with total Routhian surface and cranked shell model calculations. The presence of proton excitations in both positive- and negative-parity states has been confirmed.

PACS. 29.30.Kv X- and γ-ray spectroscopy – 23.20.Lv γ transitions and level energies – 21.60.Ev Collective models – 27.80.+w $190 \leq A \leq 219$

1 Introduction

The Pt nuclei in the $A \sim 190$ region display potential energy surfaces which are very unstable with respect to γ-deformation. Such "γ-soft" nuclei represent the best cases to study shape changes induced by the occupation of specific high-j orbitals near the Fermi surface. In contrast to the rather stable oblate-shaped Hg neighbours [1] and the predominantly triaxial-shaped heavier gold nuclei (induced by the odd proton in the $h_{11/2}$ orbital [2,3]), a variety of shapes depending on the configurations of the excited quasiparticles may be expected in platinum nuclei.

The heavy Pt nuclei have only been studied up to moderate spins using $(\alpha, x\mathrm{n})$ reactions [4–6] (even-A nuclei) and [7] (odd-A nuclei). Some features of their low-lying level spectra suggest a deviation from axial symmetry. For example, the complex low-lying positive-parity level structures in the heavy odd-mass isotopes ^{191,193}Pt can be described [7] assuming a coupling of the high-j $\nu i_{13/2}$ hole to a rotating triaxial core. Further evidence for non-axial deformation in Pt isotopes was provided by the odd-parity states. The systematically appearing semidecoupled bands built on 5^- (8^-) states in the even-mass Pt and Hg nuclei display characteristic differences which could be explained in the model of Toki *et al.* [8] assuming an axially symmetric (oblate) core for Hg but a triaxial one for Pt. In this model the important role of proton contributions to the semidecoupled bands in Pt has also been inferred.

Rotational bands built on $I^\pi = 10^-$ isomeric states have been observed in the even-mass Pt nuclei and associated with the $\nu i_{13/2}^{-1} \nu h_{9/2}^{-1}$ configuration. Structures containing this configuration were also reported for ^{191}Au [2] and ^{190,192}Au [3,9]. In the odd-mass Pt nuclei no analogous structure had been observed so far.

The present paper reports on the high-spin states in ^{191}Pt. The results extend considerably the previous level scheme [7]. Several level sequences have been identified at higher spins for the first time. The interpretation of the observed structures has been made on the basis of total Routhian surface (TRS) and cranked shell model (CSM) calculations. Very favoured structures involving an $h_{9/2}$ quasineutron hole were found to drive the nucleus towards a strongly triaxial shape at a deformation $\gamma \sim -90^\circ$. They coexist with oblate-shape structures at $\gamma \sim -60^\circ$.

2 The experiment

Excited states in ^{191}Pt were populated using the ^{186}W + ^{11}B reaction at 85 MeV with a target consisting of a stack of two 280 μg/cm^2 ^{186}W self-supporting foils. The experiment was carried out with the Eurogam-II multidetector array operating at the Vivitron accelerator in IReS

[a] e-mail: dorak@inrne.bas.bg
[b] *Present address*: CENG, IN2P3-CNRS, B.P. 120, F-33175 Gradignan cedex, France.

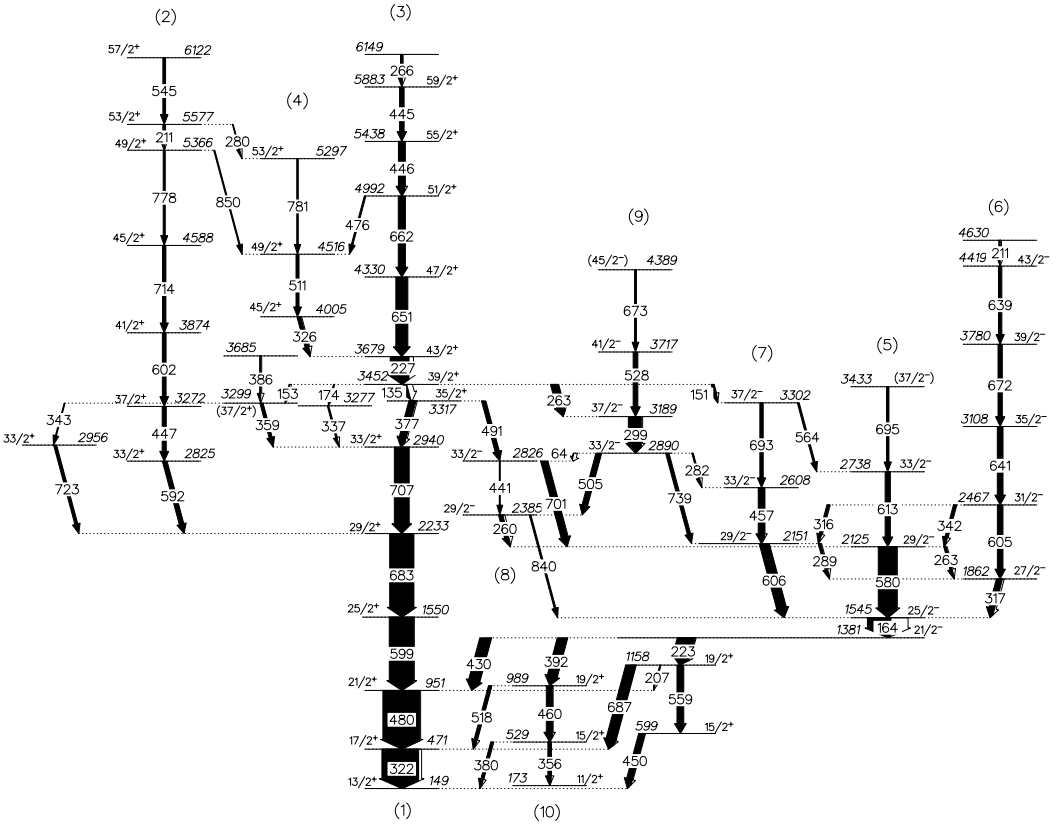

Fig. 1. Level scheme of ^{191}Pt obtained in the present work.

(Strasbourg). This array included 30 large (73%) volume Compton-suppressed Ge detectors located in rings at 22°, 46°, 134° and 158°, and 24 "clover"-type Ge detectors located close to 90° relative to the beam direction [10]. The elements of the clover detectors formed rings at 71°, 80°, 100°, and 109° with respect to the beam direction. Events were recorded when at least five unsuppressed detectors fired in prompt coincidence. A total of 9×10^8 four and higher-fold events was collected. In this experiment, which was initially designed for investigating the excited states in ^{190,191}Au produced in the xn main reaction channels, the ^{190,191}Pt nuclei were also populated in the p6n and p5n channels (4% and 1% of the events, respectively) with enough statistics to allow a detailed study of their high-spin states. The results on the high-spin level scheme of ^{190}Pt are published elsewhere [11]. The events were sorted into a E_γ-E_γ-E_γ cube with the Radware software package [12]. Setting two clean gates on low-lying gamma-transitions in ^{191}Pt allowed an efficient selection of the nucleus and a substantial extension of its level scheme. Furthermore, spectra gated by two transitions in ^{191}Pt were built at each detection angle of Eurogam-II leading to a consistent angular distribution analysis of the γ-lines. The γ-intensities of the transitions were determined from several multigated spectra obtained as a sum of the individual spectra of Ge detectors, applying appropriate intensity normalization. The statistics was not sufficient to allow for polarization measurements.

3 Results

The level scheme of ^{191}Pt had been investigated by means of (α, 3nγ) reaction by Saha *et al.* [7] and in the low-spin part by the radioactive decay of ^{191}Au [13]. The yrast sequence had been seen up to $(33/2^+)$ level at 2940 keV and identified as the favoured signature of the decoupled $\nu i_{13/2}$ band. A number of low-spin positive-parity levels has been found and interpreted as belonging to the same $\nu i_{13/2}$ family. An onset of a negative-parity sequence starting with $21/2^-$ level had been identified and its connection to the yrast band established.

The level scheme of ^{191}Pt as deduced from the present data is shown in fig. 1. We added several new sequences to the level scheme and extended it to spin $59/2^+$ in the positive-parity and $(45/2^-)$ in the negative-parity parts and up to ~ 6.1 MeV excitation energy. More than 50 new transitions have been placed in the present level scheme. A short sequence built on a 919 keV state with a tentative $(17/2^+)$ assignment reported in [7] was not populated in this experiment and is not included in the level scheme (fig. 1). Table 1 lists the transition energies, relative intensities, angular distribution coefficients and assignments into the level scheme of the ^{191}Pt observed γ-rays. Most of the transitions multipolarity and spin assignments for the new levels were inferred from the known low-spin data and the present γ-ray angular distributions. For the band-like structures at high spins we assigned $E2$ multipolarity to

Table 1. Energies, γ intensities, angular distribution coefficients, multipolarities and level assignments for transitions in ^{191}Pt observed in the present work. The intensities are obtained from double gates and normalized to a total intensity of 100 for the transitions feeding into the 951 keV yrast level.

E_γ (keV)[a]	I_γ	a_2	a_4	Multipolarity	J_i^π	→	J_f^π
64	1.8(1.0)				$33/2^-$	→	$33/2^-$
134.5	12(2)	−0.06(6)	0.06(8)	$E2$	$39/2^+$	→	$35/2^+$
151.0	7(1)	−0.40(10)	0.15(13)	$E1$	$39/2^+$	→	$37/2^-$
152.6	2.2(6)				$39/2^+$	→	$(37/2^+)$
164.0	64(5)	0.01(10)	−0.01(9)	$E2$[c]	$25/2^-$	→	$21/2^-$
173.7	1.9(7)				$39/2^+$	→	
207	1.1(7)				$19/2^+$	→	$21/2^+$
210.5	6(1)	0.31(15)	−0.03(20)	$E2$	$53/2^+$	→	$49/2^+$
210.7	3.6(1.0)	−0.09(10)	0.02(13)	$M1$ or $E1$		→	$43/2^-$
223.1	47(4)[b]	−0.23(6)	−0.14(11)	$E1$[c]	$21/2^-$	→	$19/2^+$
227.0	51(4)	0.24(10)	−0.11(7)	$E2$	$43/2^+$	→	$39/2^+$
259.8	11(2)	0.34(14)	0.24(20)	$M1$	$29/2^-$	→	$29/2^-$
262.5	6(2)	−0.19(7)	−0.13(11)	$M1$	$29/2^-$	→	$27/2^-$
263.0	21(2)	−0.25(9)	−0.02(14)	$E1$	$39/2^+$	→	$37/2^-$
266	5(1)	0.57(16)		$(E2)$		→	$59/2^+$
280	1.5(8)				$53/2^+$	→	$53/2^+$
282	3(1)	0.53(17)	0.35(25)	$M1$	$33/2^-$	→	$33/2^-$
288.9	7(2)	0.03(12)	0.35(21)	$M1$	$29/2^-$	→	$27/2^-$
298.8	35(3)	0.29(7)	−0.10(10)	$E2$	$37/2^-$	→	$33/2^-$
316	7(2)	0.08(10)	0.08(17)	$M1$	$31/2^-$	→	$29/2^-$
317.0	16(2)	−0.11(6)	−0.09(10)	$M1$[c]	$27/2^-$	→	$25/2^-$
322	Gate			$E2$[c]	$17/2^+$	→	$13/2^+$
326.1	10(2)	0.04(8)		$M1$	$45/2^+$	→	$43/2^+$
336.7	3.3(9)					→	$33/2^+$
342.4	7(1)	0.14(12)	0.00(17)	$M1$	$31/2^-$	→	$29/2^-$
343	2.5(9)				$(37/2^+)$	→	$33/2^+$
358.6	8(1)	0.23(11)	−0.2(2)	$(E2)$	$(37/2^+)$	→	$33/2^+$
376.6	19(2)	−0.03(7)	−0.08(10)	$M1$	$35/2^+$	→	$33/2^+$
385.6	4(2)	0.23(10)	−0.20(17)			→	$(37/2^+)$
392.0	29(6)[b]	−0.18(10)	0.07(8)	$E1$[c]	$21/2^-$	→	$19/2^+$
430.6	31(3)	0.44(11)	−0.11(8)	$E1$[c]	$21/2^-$	→	$21/2^+$
441	2.5(9)				$33/2^-$	→	$29/2^-$
445	13(2)	0.43(13)[d]	0.10(20)[d]	$E2$	$59/2^+$	→	$55/2^+$
446	18(2)	0.43(13)[d]	0.10(20)[d]	$E2$	$55/2^+$	→	$51/2^+$
447.2	11(2)	0.33(10)	−0.06(13)	$E2$	$37/2^+$	→	$33/2^+$
456.6	18(2)	0.40(8)	−0.10(6)	$E2$[c]	$33/2^-$	→	$29/2^-$
476	5(2)				$51/2^+$	→	$49/2^+$
480	Gate			$E2$[c]	$21/2^+$	→	$17/2^+$
490.6	12(2)	−0.10(9)	−0.05(7)	$E1$	$35/2^+$	→	$33/2^-$
504.7	15(2)	0.39(9)	−0.09(10)	$E2$	$33/2^-$	→	$29/2^-$
510.8	12(2)	0.36(10)	−0.10(12)	$E2$	$49/2^+$	→	$45/2^+$
527.6	13(2)	0.42(11)	0.05(13)	$E2$	$41/2^-$	→	$37/2^-$
545.1	7(2)	0.42(10)	−0.06(15)	$E2$	$57/2^+$	→	$53/2^+$
563.5	5(1)	0.40(11)		$E2$	$37/2^-$	→	$33/2^-$
579.6	52(4)	0.23(9)	−0.03(2)	$E2$[c]	$29/2^-$	→	$25/2^-$
591.6	12(2)	0.46(10)	−0.08(10)	$E2$	$33/2^+$	→	$29/2^+$
599.2	66(5)	0.28(9)	−0.09(11)	$E2$	$25/2^+$	→	$21/2^+$
602	10(3)	0.42(11)	−0.19(12)	$E2$	$41/2^+$	→	$37/2^+$
604.5	16(2)	0.34(5)[d]	−0.02(7)[d]	$E2$	$31/2^-$	→	$27/2^-$
605.7	29(3)	0.34(5)[d]	−0.02(7)[d]	$E2$	$29/2^-$	→	$25/2^-$
613.2	14(2)	0.28(9)	−0.29(14)	$E2$	$33/2^-$	→	$29/2^-$
638.9	9(2)	0.20(8)[d]	−0.01(11)[d]	$E2$	$43/2^-$	→	$39/2^-$

Table 1. Continued.

E_γ (keV)[a]	I_γ	a_2	a_4	Multipolarity	J_i^π	→	J_f^π
641.3	15(2)	0.20(8)[d]	−0.01(11)[d]	$E2$	$35/2^-$	→	$31/2^-$
650.9	33(3)	0.48(11)	−0.12(12)	$E2$	$47/2^+$	→	$43/2^+$
662.0	19(3)	0.20(9)	−0.10(11)	$E2$	$51/2^+$	→	$47/2^+$
671.6	12(2)	0.44(10)	0.14(15)	$E2$	$39/2^-$	→	$35/2^-$
672.7	5(1)	0.47(16)		$(E2)$	$(45/2^-)$	→	$41/2^-$
683.2	64(4)	0.34(10)	−0.07(7)	$E2$[c]	$29/2^+$	→	$25/2^+$
693.1	9(2)	0.28(9)	−0.10(11)	$E2$	$37/2^-$	→	$33/2^-$
695	6(2)				$(37/2^-)$	→	$33/2^-$
701.0	19(2)	0.24(9)	0.15(15)	$E2$	$33/2^-$	→	$29/2^-$
707.0	40(4)	0.26(9)	0.07(10)	$E2$	$33/2^+$	→	$29/2^+$
713.6	9(2)	0.45(10)	−0.20(20)	$E2$	$45/2^+$	→	$41/2^+$
723.4	8(2)	0.49(8)	−0.08(11)	$E2$	$33/2^+$	→	$29/2^+$
738.8	9(2)	0.46(13)		$(E2)$	$33/2^-$	→	$29/2^-$
778.3	6(2)	0.49(16)	−0.07(14)	$E2$	$49/2^+$	→	$45/2^+$
780.6	5(2)	0.25(14)	−0.19(24)	$E2$	$53/2^+$	→	$49/2^+$
840	4(2)				$29/2^-$	→	$25/2^-$
850	3(2)				$49/2^+$	→	$49/2^+$

([a]) The energies are accurate to ±0.5 keV, except for weak or not resolved transitions.
([b]) The intensity is obtained from the branching of the 1381 keV level.
([c]) Multipolarity known also from ref. [7].
([d]) Nonresolved multiplet. The value is obtained for the total peak.

all transitions with measured $a_2 \gtrsim 0.20$. In a few cases, the unstretched dipole character of transitions (260, 282 keV) is supported by the independent spin assignments to the respective levels. For several low-energy transitions with measured negative values of a_2 we used coincidence intensity balance results to distinguish between $M1$ or $E1$ multipolarity (see below).

Figure 2 shows examples of double-gated spectra with the observed new transitions in the positive-parity bands. Above the $29/2^+$ yrast level we found two new weaker branches one of which, band 2, develops to high spins. This band is fed predominantly from the highest spin levels and its levels below the 5366 keV state receive relatively small side feeding. At high spins the level scheme is dominated by a new very strong positive-parity structure built on the 3452 keV level (band 3) with a signature opposite to that of the yrast band (1). It depopulates by several branches to lower lying bands and levels and becomes the yrast positive-parity band above spin $37/2^+$ taking away population from the side band 2. The assignment of a spin and parity to the level at 3452 keV is obtained from the angular distributions of the 151 keV and 263 keV depopulating transitions which indicate their dipole character. $E1$ multipolarity is chosen for both transitions on the basis of the intensity balance in various gates. Thus spin-parity $39/2^+$ is assigned to the 3452 keV level. The spin-parity of the 3317 keV level is then limited to $35/2^+$ by the observed coincidences of the 135 keV transition with the 377 keV and 491 keV transitions. The coincidence intensity balance in gates allowing to compare the intensity of the 135 keV transition with that of the 377, 491 keV or their sum (*e.g.* gates 707-227 keV, 701-227 keV, 322-227 keV) is consistent with $E2$ multipolarity for the 135 keV line. This is in conflict with the small negative value of the a_2 coefficient for this transition (see table 1). We suppose that the angular distribution may be distorted by an unresolved contamination in the 135 keV line, probably of a stretched dipole character. The levels at 3299 and 3277 keV located

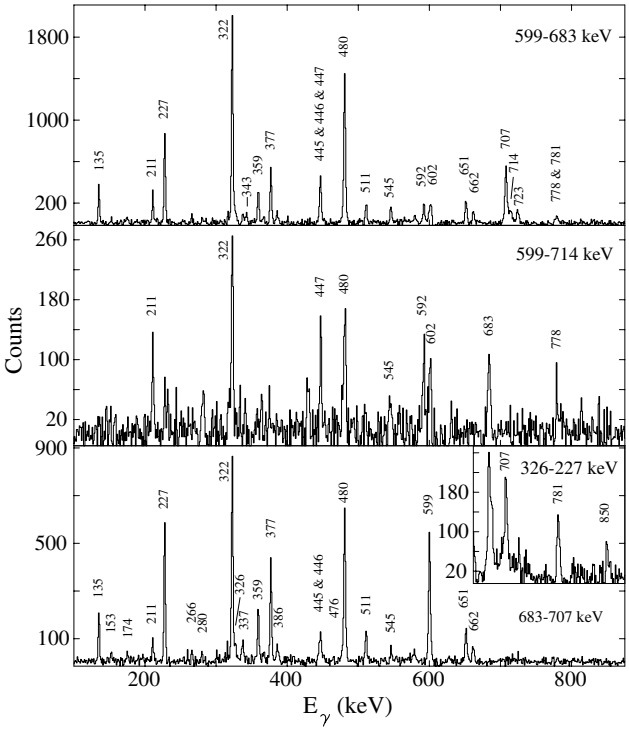

Fig. 2. Double-gated spectra showing the new transitions in the positive-parity bands.

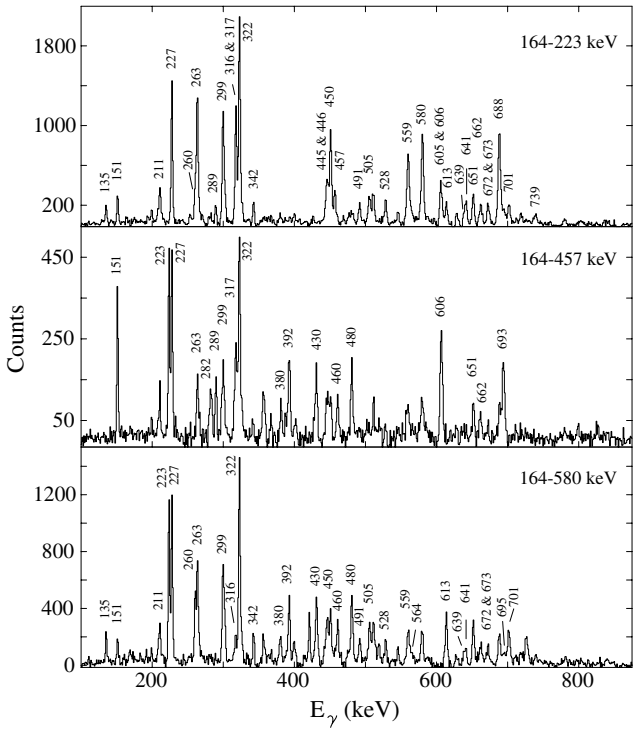

Fig. 3. Double-gated spectra showing the new transitions in the negative-parity bands.

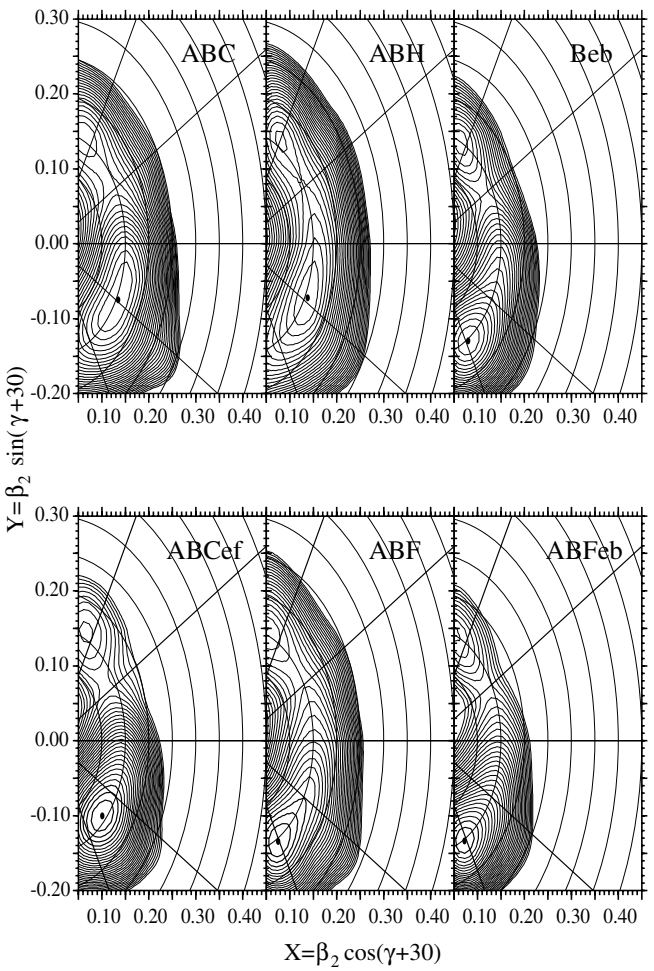

Fig. 4. TRS calculations for selected configurations in ^{191}Pt.

between the levels 3452 keV and 2940 keV should have also positive parity. For the 3299 keV level an assignment $(37/2^+)$ can be considered due to the fixed order of the 359 keV and 153 keV transitions and the angular distribution of the 359 keV transition allowing for a quadrupole type.

The negative-parity structure starting with the $21/2^-$ level at 1381 keV is populated rather strongly. Figure 3 illustrates the transitions belonging to the negative-parity sequences. We confirmed the levels at 1545, 1862 and 2125 keV established previously [7] and ordered them in bands 5 and 6. The 457 keV transition was also observed in ref. [7] and placed on top of the 2125 keV level. Our data show that the 457 keV transition is in strong coincidence with the 164 keV transition via a new 606 keV transition (see fig. 3). A weak coincidence through an unobserved 25 keV transition with the 580 keV transition is possible, however the latter is contaminated by the strong 579.6 keV γ-line of ^{191}Au and no definite conclusion could be made. In the present work we extended band 5 built on top of the 1381 keV level by two transitions and found five new transitions which form its signature partner, band 6. The 457 keV transition turned out to be a member of a new negative-parity sequence with a bandhead at 2151 keV and $I^\pi = 29/2^-$ (band 7). Bands 8 and 9 are also new structures. The existence of the 64 keV transition is deduced from the coincidence relationships between transitions in bands 5, 8 and 9. The 441 keV transition is very weak and cannot be resolved from the strong multiplet at ~ 445 keV. Its existence is confirmed indirectly from coincidences, (for example, between 491 and 164 keV lines which show a weak 260 keV γ-line). Band 9 is the yrast negative-parity sequence above spin $37/2^-$ and plays a prominent role in the de-excitation process. One can observe relationships between different negative-parity bands via interband transitions. The $(-,-1/2)$ band 6 is interconnected with both $(-,+1/2)$ bands 5 and 7 by dipole transitions close to the bandhead. Band 9 bandhead decays to bands 7 and 8. Band 8 de-excites exclusively to band 5 through strong transitions.

4 Discussion

The cores of the heavier Pt nuclei are known to be γ-soft and their shapes are expected to depend strongly on the properties of the nucleons aligning their spin along the rotation axis. For Pt nuclei in this mass region with a moderate (oblate) deformation $\beta_2 \sim 0.15$, the orbitals close to the Fermi surface are low-K orbitals from the $\nu i_{13/2}$ and $\nu h_{9/2}$ (and/or $\nu f_{7/2}$) shells and low-j orbitals from the $\nu p_{3/2}$ and $\nu f_{5/2}$ shells, as well as low-K $\pi h_{11/2}$ orbitals and low-j orbitals from the $\pi d_{3/2}$ and $\pi s_{1/2}$ shells (see fig. 4 from [2]). In order to investigate the shapes associated with these alignments, we used a set of self-consistent

Table 2. Calculated equilibrium deformations β_2 and γ from the TRS calculations for selected configurations in ^{191}Pt at relevant rotational frequencies $\hbar\omega$. The angular momentum projection on the rotational axis for neutrons I_{xn} and protons I_{xp} and the corresponding total Routhian E' are also listed.

Configuration	$\hbar\omega$ (MeV)	β_2	γ (deg)	I_{xn} ($\hbar$)	I_{xp} ($\hbar$)	E' (MeV)
vacuum $(+,0)$	0.049	0.146	−43.4			−4.93
A $(+,1/2)$	0.049	0.152	−47.4	6.3	0.2	−3.90
ABC $(+,1/2)$	0.207	0.154	−59.1	15.6	0.9	−5.24
$ABCef$ $(+,1/2)$	0.285	0.143	−82.8	19.9	10.3	−7.46
B $(+,-1/2)$	0.049	0.150	−83.8	5.5	0.1	−3.93
F $(-,1/2)$	0.049	0.160	−93.2	4.8	0.1	−3.80
ABF $(-,1/2)$	0.207	0.154	−90.6	15.5	0.7	−5.10
H $(-,1/2)$	0.049	0.151	−38.0	0.6	0.2	−3.60
ABH $(-,1/2)$	0.127	0.154	−56.8	12.6	0.7	−3.47
G $(-,-1/2)$	0.049	0.153	−32.9	1.0	0.2	−3.63
Aef $(+,1/2)$	0.127	0.142	−70.2	6.7	10.1	−3.43
Bef $(+,-1/2)$	0.127	0.143	−81.3	5.7	10.1	−3.55
Bea $(-,-1/2)$	0.089	0.151	−87.9	5.7	5.3	−3.04
Beb $(-,1/2)$	0.089	0.150	−88.2	5.7	6.1	−3.12
$ABCFH$ $(+,-1/2)$	0.207	0.148	−85.0	21.2	1.0	−4.32
$ABCFG$ $(+,1/2)$	0.207	0.150	−90.2	22.9	0.8	−4.53
$ABFeb$ $(+,-1/2)$	0.207	0.152	−91.7	15.6	6.6	−4.90
$ABFea$ $(+,+1/2)$	0.207	0.154	−91.1	15.5	5.9	−4.73

Table 3. CSM alignments calculated at $\hbar\omega = 0.30$ MeV and bandcrossing frequencies for different γ deformations in ^{191}Pt. Information on the labelling convention is also included.

			−60°	−80°	−90°
alignments ($\hbar$)					
A	$(+,+1/2)$	$\nu i_{13/2}$	6.18	6.27	6.36
B	$(+,-1/2)$	$\nu i_{13/2}$	5.03	5.27	5.37
C	$(+,+1/2)$	$\nu i_{13/2}$	3.85	4.30	4.40
F	$(-,+1/2)$	$\nu h_{9/2}$	3.34	3.90	4.17
G	$(-,-1/2)$	νj	1.69	1.52	1.56
H	$(-,+1/2)$	νj	0.70	0.60	0.60
e	$(-,-1/2)$	$\pi h_{11/2}$	5.13	5.30	5.39
f	$(-,+1/2)$	$\pi h_{11/2}$	3.67	4.26	4.36
a	$(+,+1/2)$	πj	0.41	0.43	0.49
b	$(+,-1/2)$	πj	0.66	0.75	0.83
$\hbar\omega_c$ (MeV)					
BC			0.24	0.20	0.20
ef			0.22	0.20	0.20

total Routhian surface (TRS) calculations as described in refs. [14,15]. In table 2 we list the parameters of the equilibrium shapes from TRS calculations corresponding to the vacuum configuration of the core nucleus ^{192}Pt and to selected configurations in ^{191}Pt. The theoretical quasiparticle Routhians of different parity and signature are labelled by capital letters for neutrons and by small letters for protons according to a common convention (see also table 3). TRS plots for single quasineutron configurations in ^{191}Pt and those for single quasiproton configurations in ^{191}Au at low rotational frequencies are published in [2]. Figure 4 shows the calculated deformation surfaces for selected multiquasiparticle configurations in ^{191}Pt. The following interesting features emerge from these calculations:

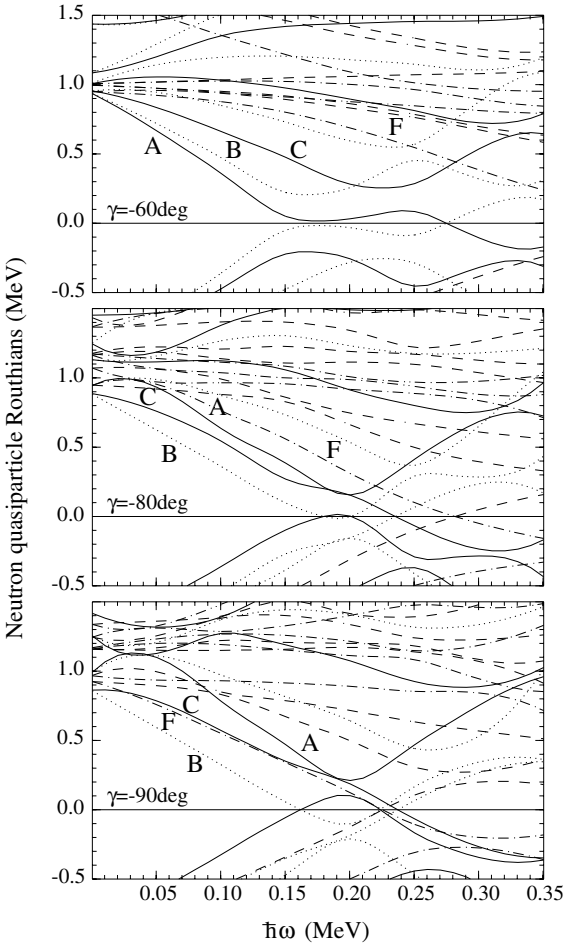

Fig. 5. Cranked shell model calculations for neutrons in ^{191}Pt. The Woods-Saxon potential with universal parameters is used. Deformation parameters of $\beta_2 = 0.15$, $\beta_4 = -0.03$ are chosen. The Routhians with $(\pi,\alpha) = (+,+1/2)$ are drown with a solid line, $(+,-1/2)$ with a dotted line, $(-,+1/2)$ with a dash-dotted line and $(-,-1/2)$ with a dashed line.

i) The energy surfaces corresponding to the vacuum configuration of ^{192}Pt and to the single-quasineutron orbitals of ^{191}Pt have soft minima with respect to the deformation parameter γ. ii) The configurations associated with the quasineutron orbitals A, B, C, D originating from the $i_{13/2}$ subshell show for the B orbital a preference for triaxial shape ($\gamma \sim -85°$) while the remaining Routhians do not influence significantly the nuclear shape. iii) The lowest negative-parity quasineutron orbital F originating from the $h_{9/2}$ subshell has a particularly strong driving force towards triaxial shape with $\gamma \sim -90°$. As can be seen in table 2 and fig. 4 all configurations containing an F quasineutron have large nonaxiallity. The next negative-parity orbitals G and H originating from low-j orbitals ($p_{3/2}, f_{5/2}$) have, on the other hand, small driving influence on the core. iv) Calculations for configurations containing quasiprotons show large triaxiality partly due to the involvement of an e $(-,-1/2)$ Routhian derived from the $h_{11/2}$ subshell which drives the shape towards $\gamma \sim -80°$ (see also ref. [2]). The TRS calculations

thus predict almost oblate ($\gamma \sim -60°$) and strongly triaxial ($\gamma \sim -90°$) shapes for the configurations in ^{191}Pt. These shape variations are expected to influence the nuclear properties such as the relative position of the orbitals and their slopes, the alignment gains, band crossing frequencies and have to be taken into account. Cranked shell model calculations were thus performed with an universal Woods-Saxon potential [16] for $\beta_2 = 0.15$, $\beta_4 = -0.03$ as obtained from the TRS calculations for deformations $\gamma = -60°, -80°$ and $-90°$. The neutron pairing gap was increased by 10% to 0.92 MeV and the proton pairing gap was kept to the predicted value of 0.69 MeV. The neutron quasiparticle Routhians are shown in fig. 5. A strong dependence on γ-deformation can be noticed for the positive-parity A, B and C Routhians. The B Routhian drops quickly, causing a signature inversion for $\gamma < -70°$. For large nonaxiallity the lowest lying positive-parity positive-signature Routhian has smaller alignment at low rotational frequency than the second lowest one. Following ref. [3] we label the Routhian with the larger alignment A for all γ-deformations and frequencies and the one with smaller alignment C. The fast dropping down of the F Routhian with increased nonaxiallity is worth noting. The aligned angular momenta for Routhians involved in the configurations of ^{191}Pt and some crossing frequencies calculated using CSM are listed in table 3. The results of the TRS and CSM calculations are used to assign configurations to the observed structures in ^{191}Pt. The experimental aligned angular momenta i and quasiparticle Routhians e' are extracted from the data using the reference parameters $J_0 = 10\,\hbar^2\,\mathrm{MeV}^{-1}$ and $J_1 = 55\,\hbar^4\,\mathrm{MeV}^{-3}$ which give zero alignment for the ground bands in the neighbouring even-even isotopes ^{190,192}Pt. It should be mentioned that $K = 0$ is used in these calculations (see ref. [2]).

4.1 The positive-parity bands

At low angular momenta the yrast band (1) is associated with the favoured signature of the decoupled $\nu i_{13/2}^{-1}$ band. Several additional positive-parity levels observed at low excitation energies were considered to belong also to the unique-parity $\nu i_{13/2}$ level family [7]. The short sequence (band 10) built on the $11/2^+$ state is the unfavoured partner. The observation of such bands at low energies in ^{191}Pt has been considered to be a consequence of the triaxial shape of the core and the location of the Fermi surface deep inside the $i_{13/2}$ neutron shell [7]. These low-spin structures have been described by Saha *et al.* [7] using the asymmetric rotor model [17]. The TRS calculations show that the occupation of the $(+,+1/2)$ orbital A is associated with a deformation $\beta_2 \sim 0.15$, $\gamma \sim -47°$ which is close to that of the core nucleus ^{192}Pt but with a stiffer minimum. The deformation predicted for the B orbital is $\beta_2 = 0.150$, $\gamma = -84°$ before the crossing. The experimental aligned angular momenta and Routhians of the positive-parity bands are shown in fig. 6. The aligned spins of $\sim 6.3\ \hbar$ and $\sim 5.2\ \hbar$ for bands 1 and 10 are very close to those in the oblate ^{191,193}Hg, which for the A configuration can be explained by the small shape differences in

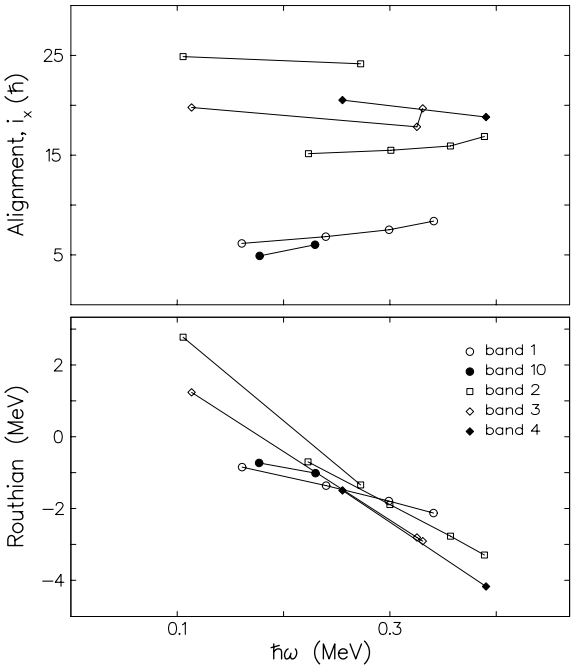

Fig. 6. The experimental alignments and Routhians for positive-parity bands in ^{191}Pt.

Pt and Hg nuclei. The first alignment is predicted by TRS to be due to a pair of neutrons which drives the nuclear shape to oblate with $\gamma = -59°$, β_2 remaining unchanged. Band 2 can be associated with the continuation of band 1 after the alignment of a pair of neutrons (ABC band). It has indeed features of an oblate band with energy spacings close to those of, *e.g.*, the yrast band of ^{192}Hg. The experimental alignment of $\sim 15.4\ \hbar$ for band 2 and the gain in alignment of $\sim 9.1\ \hbar$ with respect to the alignment of band 1 is the same as in the oblate ^{191,193}Hg nuclei [18,1] for the alignment of a BC neutron pair. These features are well reproduced by the present CSM calculations. Band 2 crosses band 1 at $\hbar\omega \sim 0.29$ MeV which is close to the frequency of the BC crossing of $\hbar\omega \sim 0.27$ MeV in ^{191,193}Hg. An additional delay of the BC crossing in ^{191}Pt may be due to the different shapes of the crossing bands (triaxial to oblate), whereas the crossing bands in the odd Hg isotopes have the same oblate shape. At $49/2^+$ the structure of band 2 changes indicating a further crossing. The aligned spin increases up to $\sim 24.8\ \hbar$. This is probably the second crossing predicted by the TRS calculations due to the alignment of a $\pi h_{11/2}^{-2}$ (ef) pair which drives the shape to $\beta_2 = 0.14$, $\gamma \sim -83°$. The gain in alignment of $9.1\ \hbar$ and the crossing frequency $\hbar\omega \sim 0.29$ MeV can be compared with the known ef crossing in ^{194}Hg where the $ABCDef$ band crosses the $ABCD$ band resulting in an alignment gain of $\sim 8.9\ \hbar$ at $\hbar\omega \lesssim 0.36$ MeV [1]. The CSM value of $25.4\ \hbar$ for the alignment of the $ABCef$ configuration in ^{191}Pt reproduces the experimental data well. The calculated crossing frequencies are lower than the experimental ones as no configuration-dependent pairing gap calculations were performed. The predicted weak dependence of the ef crossing frequency on the

γ-deformation can be noticed. The decay of band 2 into band 4 above the 5366 keV level may indicate a similarity in the structure and/or shape of these bands.

The new high-spin positive-parity structures 3 and 4 will be discussed in subsection 4.3 as well as the character of the $33/2^+$ level at 2940 keV. Another $33/2^+$ level at 2956 keV is rather isolated and no band could be established on top of it. It may be the next member of the ground band as obtained by the VMI extrapolation.

4.2 The negative-parity bands

Two negative-parity sequences built on the $21/2^-$ and $27/2^-$ $(23/2^-)$ states occur systematically in heavier odd-A Pt and Hg nuclei. They are closely related to the semidecoupled 5^- and 8^- bands in the even-even neighbours with an additional $\nu i_{13/2}$ hole coupled to the core states. In the even-even nuclei the 5^- and 8^- states are considered to be built on a two-quasiparticle configuration $\nu i_{13/2}^{-1}\nu j$, the high-j quasiparticle being decoupled from the rotational core, while the low-j one ($p_{3/2}$ or $f_{5/2}$) is strongly coupled to the core. The particular band structure depends on the deformation of the core which causes important differences for the semidecoupled bands in the predominantly oblate Hg nuclei with respect to those in Pt isotopes at low spins. The much larger 9^--7^- level spacing in the even heavy Pt nuclei has been explained in the model of Toki *et al.* [8] assuming a triaxial nuclear shape with $\gamma = 30°$ (convention $0° \leq \gamma \leq 60°$) for the semidecoupled bands of the Pt isotopes. Another difference concerns the lowering of the bandhead energy (the 5^- state) by several hundred keV in the Pt isotopes compared to Hg. It was reproduced by Toki *et al.* [8] for the even Pt nuclei by including large contributions of the proton configurations $\pi h_{11/2}^{-1}\pi j$ (πj being $s_{1/2}$ or $d_{3/2}$) as well as by reducing the proton and neutron paring gaps. Similar differences are observed between the semi-decoupled bands in the odd-mass Pt and Hg nuclei. The level spacing of the $29/2^-$ - $25/2^-$ levels of band 5 is large, 580 keV, as in ^{190,192}Pt, compared to the spacing of $\sim$ 300 keV in the ^{191,193}Hg nuclei. The bandhead $21/2^-$ lies, with respect to the $13/2^+$ level, at 1232 keV in ^{191}Pt and at $\gtrsim$ 1600 keV in ^{191,193}Hg.

Before discussing the alignments of these bands and of the new negative-parity structures we note that they have levels of the same spin with close excitation energies, *e.g.* the two $29/2^-$ levels in bands 5 and 7 are separated by only 26 keV and the two $33/2^-$ levels in bands 8 and 9 are 64 keV apart. Such a close proximity in excitation energy may lead to an interaction between these states and thus deform the experimental alignments.

The experimental aligned spins and Routhians for the negative-parity bands are displayed as a function of rotational frequency in fig. 7. We can see that the initial alignments of the negative-parity bands are about 11 $\hbar$, 13 $\hbar$ and 16 $\hbar$ for bands 5/6, 7 and 9, respectively. The alignment of band 6 is observed only in the high-frequency region. The 11 $\hbar$ alignment for band 5 is smaller than expected if its configuration were pure quasineutron as in the odd-mass Hg isotopes with the $\nu i_{13/2}$ pair fully aligned. In accordance with the expected quasiproton contribution to the structures of the semidecoupled bands, the TRS calculations show that the $\nu i_{13/2}^{-1} \otimes \pi h_{11/2}^{-1}\pi j$ configurations have energetically lower Routhians. Moreover, since the $\pi h_{11/2}^{-1}$, (e) quasiproton drives the shape towards a triaxial shape ($\gamma \sim -80°$) at which signature inversion in the positive-parity Routhians A and B occurs, (see fig. 5) the lowest-lying Routhians for the semidecoupled bands are expected to be Beb $(-,-1/2)$ and Bea $(-,+1/2)$. TRS calculations predict a triaxial minimum at $\gamma \sim -88°$ for the Beb and Bea configurations which may contribute to the structure of the semidecoupled bands 5 and 6. (The Aea, Aeb Routhians lie higher by $\gtrsim$ 200 keV.) At this γ deformation, the most likely neutron components of the semidecoupled bands 5 and 6 are the BCH and BCG configurations, respectively, (see fig. 5). The alignments of the Beb, Bea, BCH and BCG configurations (11.6, 11.3, 10.2 and 11.1 $\hbar$, respectively) calculated by the CSM at the relevant deformations (see table 3) are in a good agreement with the experimental alignments for bands 5/6. This result can be considered a confirmation by the TRS and CSM calculations for the previously suggested [8] proton contribution to the structure of the semidecoupled bands in Pt nuclei. In the oblate ^{191,193}Hg the experimental alignment of the semidecoupled bands is about 12.7–13.0 $\hbar$ and correspondingly the assigned configurations are ABF, ABE in the notation of refs. [18,19], F and E being the lowest negative-parity Routhians corresponding to the low-j orbitals. An alignment of $\sim$ 12.6 $\hbar$ obtained for band 7 suggests an ABH configuration. The TRS calculations predict an oblate deformation for the ABH configuration ($\gamma \sim -57°$, $\beta_2 \sim 0.15$). At this deformation the CSM alignment is 11.9 $\hbar$ (see table 3)

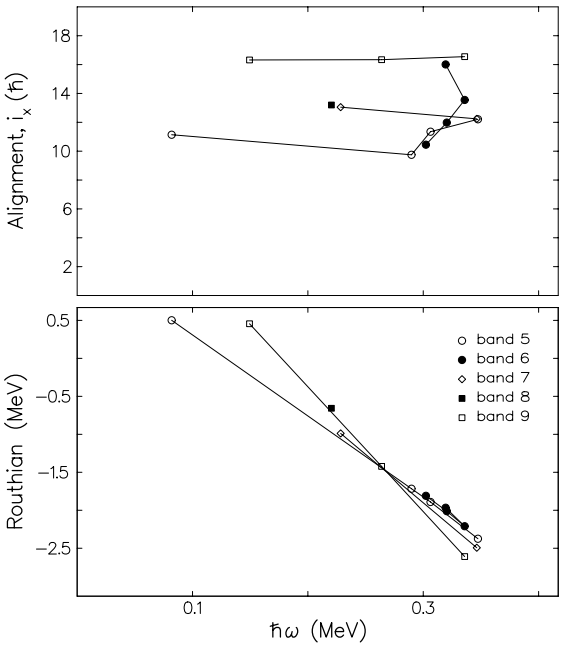

Fig. 7. The experimental alignments and Routhians for negative-parity bands in ^{191}Pt.

reproducing the experimental value. This band is probably of a predominantly neutron configuration similar to the semidecoupled bands in the odd-mass Hg nuclei.

The high alignment ($i \sim 16.2\ \hbar$) and the steep Routhian of band 9 allows us to propose a configuration $\nu h_{9/2}\nu i^{-2}_{13/2}$ for it. TRS calculations predict a deformation $\gamma \sim -91°$, ($\beta_2 \sim 0.154$) for the ABF configuration. A band of ABF' configuration in the notation of ref. [18] where F' corresponds to an $h_{9/2}$ quasineutron has been identified also in ^{191}Hg with an alignment of 15.0 $\hbar$ and a deformation $\beta_2 = 0.13$, $\gamma \sim -80°$. In ^{191}Hg the triaxial minimum developes at higher frequencies. In ^{191}Pt, the alignment of band 9 is higher than that of band 2. This can be understood by the CSM calculations which take into account deformation parameters of each configuration. An alignment of 15.1 $\hbar$ (15.9 $\hbar$) is obtained for the $ABC(ABF)$ configuration from CSM diagrams at $\gamma = -60°$ ($\gamma = -90°$), respectively, in good agreement with the experimental values. This rather extreme case of bands with strongly differing deformations coexisting in the same nucleus illustrates the importance of the shape on the nuclear properties. To assign configuration to the structure labelled (8) we note its relation to band 9. Indeed, the ratio of the reduced transition probabilities $B(E2; 505\,\mathrm{keV})/B(E2; 739\,\mathrm{keV}) = 11.1$ implies some similarity of the intrinsic structures of bands 9 and 8. Taking into account also the alignment of $\sim 13\ \hbar$ for the only point of structure 8 we assign to it a configuration BCF. The deformation calculated by TRS for this configuration ($\beta_2 = 0.152, \gamma = -89.3°$) is very close to the deformation of the ABF configuration. In the CSM diagram for $\gamma = -90°$ (fig. 5) we observe that the BCF configuration is yrast at low frequencies, but may exchange with the ABF configuration at higher frequency ($\hbar\omega \gtrsim 0.2\,\mathrm{MeV}$) due to a steeper slope of the A orbital and its interaction with the C orbital. This may explain the experimental observation that band 8 does not develop to high spins but switches to band 9. The calculated CSM alignment of 14.0 $\hbar$ for the BCF configuration is in qualitative agreement with the experimental one for band 8. The above mentioned structures can be considered as an analogue to the bands built on the isomeric 10^-, (11^-) states in the even-even ^{190,192}Pt nuclei [4,6] with the $\nu i^{-1}_{13/2}\nu h^{-1}_{9/2}$ configuration. Coupled to the odd proton, this configuration produces the $31/2^+$ isomers in the odd Au isotopes [2]. Recently, isomeric structures involving the $\nu i^{-1}_{13/2}\nu h^{-1}_{9/2}$ quasineutrons have been observed in the odd-odd ^{190,192}Au nuclei [9]. In the present work we observe this structure for the first time in an odd-N platinum isotope.

4.3 The structure built on the $39/2^+$ state at 3452 keV

The depopulation of the 3452 keV level, on top of which a new high-spin structure is built, is rather fragmented and proceeds towards the negative-parity bands 7 and 9 to the $35/2^+$ level at 3317 keV and to two additional positive-parity levels. No decay to the ABC band 2 was observed. The decay pattern and the excitation energy of the $39/2^+$ level suggest that it has a five-quasiparticle configuration with components from the $\nu i_{13/2}$, $\nu h_{9/2}$ and low-j subshells. A similar structure built on the 14^+ (3415 keV) and 17^+ (3808 keV) states has also been identified in ^{190}Pt [11]. It has been interpreted in [11] as a combination of the semidecoupled (5^-, 8^-) and the isomeric (10^-) structures with the configuration $\nu i^{-2}_{13/2}\nu h^{-1}_{9/2}\nu j$. Correspondingly, the configuration in ^{191}Pt is $\nu i^{-3}_{13/2}\nu h^{-1}_{9/2}\nu j$. The branch starting with the $45/2^+$ state at 4005 keV (band 4) may be the other signature of this configuration. Note that the energies of the band heads of bands 3 (4) are close to the sum of the band-head energies of the semidecoupled bands 1381 keV (1862 keV) with the 2385 keV level of band 8 (with respect to the $13/2^+$ level at 149 keV). From fig. 6 we can see that the Routhian of band 3 is yrast with respect to that of band 2 and crosses the ground band A at $\hbar\omega \sim 0.26\,\mathrm{MeV}$, which is lower than the $A \to ABC$ crossing. The favoured position of band 3 may be due to a combined effect of the proton contribution in the component coming from the semidecoupled structure on one hand, and from the strong influence of the $h_{9/2}$ quasineutron, on the other. The proton contribution ($\nu i^{-2}_{13/2}\nu h^{-1}_{9/2} \otimes \pi h^{-1}_{11/2}\pi j$) to bands 3 and 4 is reflected in their signatures for the $ABFeb$ $(+,-1/2)$ and $ABFea$ $(+,+1/2)$ configurations. They lie lower than the possible neutron components $ABCFH$ and $ABCFG$ (cf. table 2). Pure neutron bands belonging to the latter configurations are identified in ^{193}Hg and ^{191}Hg, respectively, and labelled $ABCEF'$ [18,19][1]. They lie much higher in energy than bands 3 and 4 and decay predominantly to the positive-parity bands. The TRS calculations predict large triaxial deformations of $\gamma \sim -90°$ for both the pure neutron and mixed proton-neutron configurations (see table 2) in ^{191}Pt. The bands in the Hg isotopes are characterised by smaller nonaxiallity, $\gamma \sim -80°$. The experimental alignments of $\sim 20.0\ \hbar$ for bands 3 and 4 are smaller than expected if compared to the alignment of band 9. Since bands 3 and 4 are of mixed composition, a better comparison can be made with the experimental alignment of $\sim 11\ \hbar$ for band 5 added to the experimental alignment of $\sim 9\ \hbar$ for the 11^- (AF) band in ^{192}Pt, resulting in a value of $\sim 20\ \hbar$. The similarity of the shapes of band 2, above the suggested quasiproton crossing, and band 4 may explain the connecting transitions between these bands.

The nature of the $33/2^+$ state at 2940 keV remains to be discussed. The existence of three $33/2^+$ states in ^{191}Pt lying within 130 keV should be noticed. They can be compared to the three close-lying 10^+ states in ^{190}Pt (and two in ^{192}Pt) [4,6]. Piiparinen *et al.* [5] suggested an equal importance of $\nu i^{-2}_{13/2}$ and $\pi h^{-2}_{11/2}$ excitations in the alignment process in these Pt nuclei. Thus two of the 10^+ states were associated with these excitations and the third one (in ^{190}Pt) with the next member of the ground band. The assignment of the $\pi h^{-2}_{11/2}$ configuration to the

[1] Note that the signature of the E orbital is $-1/2$, $+1/2$ in refs. [18] and [19], respectively

lowest-lying 10^+ states in ^{190,192}Pt has been questioned in ref. [6]. The present data on ^{191}Pt may present more convincing evidence for the existence of such proton excitations. We suggest that the most strongly populated $33/2^+$ state at 2940 keV is based on the $\pi h_{11/2}^{-2}$ excitation coupled to a $\nu i_{13/2}^{-1}$ quasineutron (Aef). It is populated from structure 3 via several paths. The $35/2^+$ level at 3317 keV might also belong to the same configuration (Bef) corresponding to observed odd-spin positive-parity states in the alignment region of the even-even Pt. The TRS calculations predict a deviation from axial shape for the configurations Aef and Bef, (see table 2), which is induced by the e quasineutron. The similarity with the shape of structure 3(4) may be responsible for the preferred decay from the latter into these levels instead of into the oblate $\nu i_{13/2}^{-3}$ band 2.

5 Conclusions

In the present work the level scheme of the heavy odd nucleus ^{191}Pt has been studied for the first time to high spins. Several new band structures have been identified and the previously known structures have been extended to higher spins. Total Routhian surface calculations were carried out to study the shapes of different bands. Three- and five-quasiparticle structures with large negative deformations ($\gamma \sim -90°$) due to an excited $h_{9/2}$ quasineutron are found to coexist with almost oblate bands at comparable excitation energies. The CSM calculations reproduce well the experimental alignments of the bands at corresponding deformations. A sizable contribution of proton configurations suggested previously has been confirmed for the semidecoupled bands and found in the new high-spin structures.

The EUROGAM project was funded jointly by the IN2P3 (France) and the EPSRC (UK). We are grateful to H. Folger and his collaborators at the GSI Target Laboratory for their high-quality targets and to the team of the Vivitron (IReS, Strasbourg) for providing excellent beams. Two of us T. K. and A. M. thank the CSNSM for hospitality and financial support.

References

1. H. Hübel *et al.*, Nucl. Phys. A **453**, 316 (1986).
2. E. Gueorguieva *et al.*, Phys. Rev. C **68**, 054308 (2003).
3. E. Gueorguieva *et al.*, Phys. Rev. C **69**, 044320 (2004).
4. J.C. Cunnane *et al.*, Phys. Rev. C **13**, 2197 (1976).
5. M. Piiparinen *et al.*, Phys. Rev. Lett. **34**, 1110 (1975).
6. S.A. Hjorth *et al.*, Nucl. Phys. A **262**, 328 (1976).
7. S.K. Saha *et al.*, Phys. Rev. C **15**, 94 (1977).
8. H. Toki *et al.*, Nucl. Phys. A **279**, 1 (1977).
9. E. Gueorguieva *et al.*, Phys. Rev. C **64**, 064304 (2001).
10. G. Duchêne *et al.*, in *Proceedings of the Workshop on Large Gamma-Ray Detector Arrays, Chalk River, Canada, 1992*, AECL 10613 (1992); P.M. Jones *et al.*, Nucl. Instrum. Methods Phys. Res. A **362**, 556 (1995).
11. E. Gueorguieva, PhD Thesis No. 5796, Université Paris-Sud and University of Sofia (1999).
12. D.C. Radford, Nucl. Instrum. Methods Phys. Res. A **361**, 297 (1995).
13. M. Piiparinen *et al.*, Nucl. Phys. A **265**, 253 (1976).
14. W. Nazarewicz, G.A. Leander, J. Dudek, Nucl. Phys. A **467**, 437 (1987).
15. R. Wyss, W. Satula, W. Nazarewicz, J. Dudek, Nucl. Phys. A **511**, 324 (1990).
16. J. Dudek, Z. Szimaǹski, T. Werner, Phys. Rev. C **23**, 920 (1981).
17. J. Meyer ter Vehn, Nucl. Phys. A **249**, 111; 141 (1975).
18. D. Ye *et al.*, Nucl. Phys. A **537**, 207 (1992).
19. N. Fotiades *et al.*, J. Phys. G **21**, 911 (1995).